Vascular defects and spinal cord hypoxia in spinal muscular atrophy

Vascular defects and spinal cord hypoxia in spinal muscular atrophy

Running Head: Depleted vasculature and hypoxia in SMA

Somers, E[2,3] BSc, PhD, Lees, RD[2] BMedSci, Hoban; K[2] BSc, Sleigh, JN[4] MBiol, DPhil, PhD; Zhou, H[5] PhD; Muntoni, F[5] MD; Talbot, K[4] DPhil, Gillingwater, TH[2,3] BSc, PhD, Parson, SH[1,3]* BSc, PhD

[1] Institute of Medical Sciences, University of Aberdeen, Foresterhill, Aberdeen, AB25 2ZD, UK

[2] Centre for Integrative Physiology, University of Edinburgh, Edinburgh, EH8 9XD, UK

[3] Euan MacDonald Centre for Motor Neurone Disease Research, University of Edinburgh, Edinburgh, EH8 9XD, UK

[4] Nuffield Department of Clinical Neurosciences, University of Oxford, John Radcliffe Hospital, Oxford OX3 9DU, UK

[5]Dubowitz Neuromuscular Centre, Institute of Child Health, University College London, London WC1N 1EH, UK

Corresponding Author:

Simon H. Parson, Suttie Centre, University of Aberdeen, Foresterhill, Aberdeen, AB25 2ZD, UK

Title: 121 Characters

Running Head: 34 characters

Abstract: 239 words

Introduction: 343 words

Discussion: 1767 words

Body: 5691 words

Figures: 6

Colour figures: 3

Tables: None

Abstract

Objective

Spinal Muscular Atrophy (SMA) is a major inherited cause of infant death worldwide. It results from mutations in a single, ubiquitously expressed gene (*SMN1*), with loss of lower motor neurons being the primary pathological signature. Systemic defects have also been reported in SMA patients and animal models. We investigated whether defects associated with the vasculature contribute to motor neuron pathology in SMA.

Methods

Development and integrity of the capillary bed was examined in skeletal muscle and spinal cord of SMA mice, and muscle biopsies from SMA patients and controls, using quantitative morphometric approaches on immunohistochemically-labelled tissue. Pimonidazole hydrochloride-based assays were used to identify functional hypoxia.

Results

The capillary bed in muscle and spinal cord was normal in pre-symptomatic SMA mice (post-natal day 1), but failed to match subsequent post-natal development in control littermates. At mid- and late-symptomatic time-points the extent of the vascular architecture observed in two distinct mouse models of SMA was ~50% of that observed in control animals. Skeletal muscle biopsies from human patients confirmed the presence of developmentally similar, significant vascular depletion in severe SMA. Hypovascularity in SMA mouse spinal cord was accompanied by significant functional hypoxia and defects in the blood-spinal cord barrier.

Interpretation

Our results indicate that vascular defects are a major feature of severe forms of SMA, present in both mouse models and patients, resulting in functional hypoxia of motor neurons. Thus, abnormal vascular development and resulting hypoxia may contribute to the pathogenesis of SMA.

Introduction

Spinal muscular atrophy (SMA) is an inherited, monogenic condition, resulting from homozygous deletion of the survival of motor neuron (*SMN1*) gene [1]. The gene was originally named a the assumption that it is specifically required for maintenance and survival of motor neurons, thereby explaining the primary lower motor neuron-associated phenotypes of affected children. In addition, many recent studies have highlighted the importance of SMN protein for the normal development and maintenance of a range of other cell types, tissues and organs in SMA. What is particularly striking, is the discovery of widespread tissue and organ pathology beyond the neuromuscular system [2, 3]. These systemic pathologies may manifest sub-clinically in human SMA patients [4, 5]. However, similar defects have been unmasked when therapies specifically targeting the motor system resulted in significant improvement of motor skills, but failed to rescue overall disease severity in SMA mice [6-8]. Furthermore, recent work using peripherally-targeted rescue strategies has demonstrated that therapies which specifically do not modulate SMN protein levels in the central nervous system (CNS) are still able to significantly ameliorate disease severity in SMA mice [9, 10].

The role that the cardiovascular system, and blood vessels in particular, plays in SMA pathogenesis remains unclear. However, cardiac defects have been described in SMA patients as well as animal models [4, 5, 11], and disrupted capillary networks are reported in skeletal muscle from SMA mice [12]. Moreover, vascular defects have been linked to the pathogenesis of other neurodegenerative conditions such as Alzheimer's disease [13], and diseases where motor neurons are targeted, such as

amyotrophic lateral sclerosis (ALS) [14]. Such serious and significant defects in the capillary bed are likely to impact upon the delivery of oxygen to tissues, and potentially also to the development and function of myriad systems in the body. Whether damage to the vasculature and microcirculation within the spinal cord occurs in SMA remains unknown. Here, we combined analysis of established mouse models of severe forms of SMA with muscle biopsies from severe SMA patients to address these questions.

Materials and Methods

Mice: 'Taiwanese' SMA mice (Jackson Labs strain no. 005058) on a congenic FVB background were maintained as breeding pairs ($Smn^{+/-}$ x $Smn^{-/-};SMN2^{tg/tg}$) pairs under standard SPF conditions in animal care facilities in Edinburgh. Offspring were either homozygous knockout for endogenous *Smn* ($Smn^{-/-};SMN2^{tg/0}$), referred to as SMA or heterozygous for *Smn* knockout ($Smn^{+/-};SMN2^{tg/0}$), referred to as 'Control'. SMA mice therefore carry two *SMN2* copies on one allele on a null murine *Smn* background [15]. Retrospective genotyping for this strain was carried out using standard PCR protocols [16].

'Delta 7' SMA mice on a congenic FVB background were maintained as heterozygous $SMN2^{+/+};SMN2\ \Delta 7^{+/+};Smn^{+/-}$ (Jackson labs strain no. 005025) breeding pairs. Offspring were either; *Smn* KO: $SMN2^{+/+};SMN\Delta7^{+/+};Smn^{-/-}$, referred to as 'SMA' or *Smn* heterozygous; $SMN2^{+/+};SMN\Delta7^{+/+};Smn^{+/-}$, referred to as 'Control'. Some offspring are homozygous wild-type for *Smn* and were not used in the study. Mice were maintained in animal care facilities and genotyped in Oxford as previously reported [17]. In each case the morning of the day on which a litter was found was designated P0. All animal procedures and breeding were performed under licensed authority of the UK Home Office, and in accordance with local institutional guidelines.

Taiwanese SMA-affected mice are first distinguishable from control littermates at P6/7 by reduction in weight and early weakness. They are typically sacrificed at the humane endpoint of P10-11 due to severe paralysis. Delta 7 SMA-affected mice are first distinguishable from control littermates at P7 by reduction in weight and early

weakness. They are typically sacrificed at the humane endpoint of P13-15 due to severe paralysis.

Mouse tissue collection: Male and female offspring were utilised in this study, as preliminary work indicated no differences between the sexes. All mice were sacrificed by intraperitoneal injection of sodium pentobarbital. Whole spinal cord-containing vertebral columns and proximal forelimbs were rapidly dissected and fixed in 0.1M phosphate buffered saline (PBS) containing 4% paraformaldehyde. Tissue was cryoprotected in a 50:50 solution of OCT and 30% sucrose prior to freezing on dry ice. Sections were cut at 10 µm from the proximal forelimbs (shoulder to elbow) and thoracic vertebral column at 14µm on a cryostat (3080 LeicaCM). Sections were selected at regular intervals from each for immunohistochemical analysis.

SMA patient and control individual skeletal muscle biopsies:

Studies on muscle biopsies from SMA patients (age range 1-34 months old, *n*=7) and control patients (age range 0.3-36 months old, *n*=9) were approved by the NRES Committee East of England Institutional Ethical Committee and conducted under the Declaration of Helsinki. Patients' personal information was encoded to protect their identity, and written informed consent obtained by the patient or the responsible guardian. All patients presented in this study have a clear clinical and pathological diagnosis of SMA (data not shown). Control muscle biopsies were from individuals with no neuromuscular or vascular diseases.

Patient biopsy immunohistochemistry

Cryosections from muscle biopsies were cut at a thickness of 7 µm for immunohistochemistry. Muscle fibres were stained with rabbit polyclonal anti-Laminin primary antibody (Sigma L9393: 1:200) and blood vessels in muscle biopsies were stained with mouse monoclonal anti-CD31/ PECAM-1 primary antibody (SeroTec MCA1738: 1:100). Double staining of Laminin and CD31/ PECAM-1 was visualized with Alexa Fluor 488 goat anti-Rabbit IgG (H+L) and Alexa Fluor 594 goat anti-Mouse IgG (H+L) (Life Technologies: 1:500). Sections were mounted in Hydromount mounting medium (National Diagnostics, England). Images were digitally captured using Metamorph software.

Mouse immunohistochemistry: Muscle sections from throughout the proximal forelimb were stained with Rhodamine-labelled *Griffonia simplicifolia* Lectin-1 (GSL-1: Vector Laboratories RL-1102: 1:100) to label the capillary bed. Some sections were double labeled with rabbit polyclonal anti-alpha smooth muscle Actin primary antibody (a-SMActin: abcam ab5694: 1:250), visualized with fluorescein-labelled polyclonal swine anti-rabbit immunoglobulin (Jackson ImmunoResearch Laboratories Inc.: 1:40) to stain smooth muscle and mounted in Mowiol.

Spinal cord sections were stained with goat anti-mouse PECAM-1 primary antibody (R&D Systems AF3628 at 1:750). After washing, slides were incubated with donkey anti-goat Cy3-conjugated secondary antibody (Jackson ImmunoResearch Laboratories Inc. at 1:250). After PECAM-1 staining, some slides were incubated overnight in SMI-32 primary antibody (a gift from Professor Siddharthan Chandran, University of Edinburgh) at 1:500 and visualized with donkey anti-mouse Alexafluor

488-conjugated secondary antibody (Dako) at 1:250. Slides were then washed and mounted as above.

Additional spinal cord sections were stained with, either rabbit anti-mouse aquaporin-4 (AQ-4: Abcam ab125049), rabbit anti-mouse claudin-5 (CL-5: Abcam ab59720) or rabbit anti-mouse zona occludens-1 (ZO-1: Abcam ab53765) primary antibodies, all at a concentration of 1:100. Each was visualized with a swine anti-rabbit FITC-conjugated secondary antibody (Dako: 1:40). Following this, capillaries were labeled with GSL-1, as described above.

Labeling of hypoxic tissue with pimonidazole hydrochloride

Entire litters of P5 Taiwanese severe model SMA mice were injected with the hypoxia marker pimonidazole hydrochloride (PIMO). PIMO diffuses effectively in tissue including the CNS [18], is retained in hypoxic cells, and can be labeled with antibodies to mark neurons in experimental hypoxia [19].

A single 60mg/kg dose of PIMO was administered via intraperitoneal (IP) injection. After injection mice were returned to their cage with their parents for 1 hr, during which time the mice were closely monitored. In this hour, PIMO was delivered systemically to all body tissues via the bloodstream. In mice, PIMO has a plasma half-life of ~25 min [20], and is cleared by the kidneys [18]. Thus, experimental durations of an hour or longer between injection and sacrifice allow for the systemic distribution of PIMO and its subsequent clearance from the plasma. 90 min after PIMO injection, Taiwanese SMA mice and control littermates were sacrificed by an overdose of anaesthetic administered via IP injection of sodium pentabarbitol (Euthenal). Mice were sacrificed in the order they were initially injected with PIMO. Each injection

was timed to ensure that each animal was exposed to PIMO for an equal amount of time and given the same time to clear residual unbound PIMO from the plasma. At the time of tissue collection, PIMO will already be bound to proteins in any hypoxic cells in the body tissues. During harvesting, tissue becomes anoxic, but the very low levels of PIMO remaining in the plasma at the time of collection should prevent any PIMO binding as a result of dissection anoxia. To further ensure this, dissections of spinal cord were performed rapidly with tissues being collected and fixed in <5 min. Nissl co-staining was also carried out on sections, to identify grey and white matter regions of the spinal cord, using a 0.2% solution of cresyl fast violet (CFV).

Imaging and Quantification

All images were captured using a chilled CCD camera (Hammamatsu C4742-95) using OpenLab image capture software on an Olympus IX71 microscope.

Muscle capillary density (mouse): was calculated for the group of muscles visible in sections through the proximal forelimb; for each muscle, six images at x20 magnification were collected. Over 1000 evenly distributed images were captured from the centre and at 90^{o}, 180^{o} and 270^{o} to a vertical line drawn through the centre of the muscle toward the periphery. Capillary density as a percentage of muscle area was calculated [12]. The same images were used to calculate the ratio of capillaries to muscle fibers (C:F), from counts of the numbers of muscle fiber and capillary profiles wholly present in each image.

Intramuscular arterioles: were analysed in vessels that expressed α-SMActin; the diameters of both the vessel and the smooth muscle, standardised to a circle, were calculated using the formula: $diameter(\mu m) = 2(\sqrt{\frac{area(\mu m)}{\pi}})$. A ratio of vessel

diameter/smooth muscle diameter (v/m) then generated an arbitrary value for each vessel representing the thickness of the outer layer of smooth muscle relative to the vessel diameter.

Spinal cord capillary density: was calculated from three sections per slide from a minimum of three slides for each mouse. Spinal cords were divided into dorsal/ventral and left/right, and adjacent CFV-stained slides used to segment white and grey matter. Within each quadrant, three radial lines of 40x images, originating from the central canal and extending to the edge of the cord, were captured. The percentage vessel area was then calculated as for skeletal muscle, and blind to genotype.

Tissue hypoxia: was analysed by counting cells double-labeled for CFV (a neuronal marker) and DAB (a marker of hypoxia) in spinal cord ventral horn and by calculating the proportion of DAB (hypoxic) stained tissue in sections of skeletal muscle.

Muscle capillary density (human): was analysed from 3-9 (mean=5) non-consecutive sections per muscle biopsy, which were photographed at x40 magnification and quantified to calculate C:F ratio as indicated above for mouse.

Statistical analysis: All data were collected using Microsoft Excel software. Graphs were generated and statistical analyses performed using GraphPad Prism software. Bar charts represent mean ± s.e.m. and scatter plots show data points and mean values. Statistical significance was considered to be $p<0.05$. Statistical tests used are detailed in the figure legends.

Results

Given the evidence for pathology outside the nervous system in SMA, we investigated the vascular system and specifically the capillary bed of clinically-relevant, proximal skeletal muscles and spinal cord in mice and skeletal muscle biopsies from type 1 SMA patients. We set out to determine if blood supply to motor nerve terminals in skeletal muscle or motor neuron cell bodies in spinal cord is compromised and therefore potentially significant in the aetiology of SMA.

Vasculature is aberrant in post-natal SMA proximal skeletal muscle

First, we extended previous studies detailing significant defects in muscle capillaries in trunk muscles[12], by demonstrating that there are parallel significant vascular defects in clinically-relevant, proximal, forelimb muscles at a symptomatic time-point (P8) in the Taiwanese mouse model of severe SMA.

A marked decrease in the density of intra-muscular capillaries (GSL-1 staining) was immediately apparent in transverse sections of multiple, individual skeletal muscles from proximal forelimbs in SMA mice (Fig 1A,B) compared with control littermates. As a percentage of cross sectional area, muscle from SMA mice was less than half as capillary-dense as control littermates (Fig 1C). Closer observation showed that many muscle fibers were no longer adjacent to capillaries in SMA muscles (Fig 1B). Therefore we next calculated the number of capillary profiles per muscle fiber profile, which is perhaps a more informative functional measure of perfusion distances and controls for bias introduced by variations in muscle fiber diameter, as occur in neuromuscular wasting diseases such as SMA. The capillary/muscle fiber ratio in SMA mice was only 40% of that in control littermates (Fig 1D), confirming

skeletal muscle hypovascularity in SMA. Larger arterioles, identified as α-Smooth Muscle Actin-(α –SMA) expressing vessels, appeared morphologically normal and mature We then checked if these intra-muscular arterioles were structurally normal and the mean caliber of intramuscular arterioles was not significantly different between SMA: 1.90µm and littermate control: 1.64µm mice, (NS P>0.05 unpaired, two-tailed *t*-test) and mature, as the ratio of vessel caliber (v) to the surrounding smooth muscle diameter (m) v/m was not significantly different between SMA: 0.738 and control littermate: 0.753 mice, (NS P>0.05 unpaired, two-tailed *t*-test) but were reduced in number in SMA mice: 57% compared to control littermates (Fig 1E). Thus, there were significantly fewer capillaries (small vessels including arterioles and venules) and fewer larger and mature, intramuscular arterioles in clinically-relevant, proximal forelimb muscles in Taiwanese severe SMA mice at a symptomatic time-point. Therefore, diffusion distances were increased and perfusion to muscle fibers and motor nerve terminals was likely compromised.

Aberrant vasculature is also present in skeletal muscle from human SMA patients

We were particularly interested to determine if similar vascular changes were present in SMA patients. To this end skeletal muscle biopsies from 7 type I/II patients and 9 controls were obtained, immunostained and analysed in an identical manner to the mouse samples. As was seen in mouse models, there were no differences in vascularity immediately after birth, but with increasing development, dramatic discrepancies became apparent. Muscle from control children showed a steady increase in C:F ratio from 0.1:1 at 0.5 months to 0.8:1 at 36 months (Fig 2A,C), which approaches a mature ratio of >1.0:1 [21, 22]. In contrast, biopsies from Type I/II

severe patients showed a failure to develop beyond the situation at birth, with a ratio of 0.09:1 at 1 month and 0.08:1 at 33 months (Fig 2A,C). By 33/36 months of age there was a tenfold difference in capillary: fibre ratio between control and SMA muscle biopsies. Regression analysis of the data shows a clear and significant diference in the rate of vascularisation between control and SMA biopsies (Fig 2C). This results in muscle fibres being much more distant from capillaries at 33/36 months in SMA compared with control muscles (Fig 2B).

These data demonstrate comparable vascular defects, and in particular an apparent falure to develop significantly after birth in severe SMA patients, directly analagous to those described in severe mouse models of SMA.

Post-natal development of spinal cord vasculature in wild-type mice

We next turned our attention to the spinal cord, in order to establish whether the loss of motor neuron cell bodies that occurs in SMA also correlates with vascular changes. Surprisingly, post-natal development of spinal cord vasculature in the mouse has not been consistently or clearly described in the literature. Therefore, we first established the normal parameters for capillary development in the post-natal spinal cord of wild-type C57Bl mice to establish baseline data. In very young animals and as a percentage of spinal cord cross-sectional area, capillaries were sparse (P3), but progressively increased in density (Fig 3A) and caliber (Fig 3B) during the first 3 weeks of post-natal development. Capillary density in the grey and white matter was similar at P3, began to increase in grey matter at P7, was significantly greater by P14, and was more than double that in white matter by P21 (Fig 3C). Over this 3 week period, capillary density had doubled in white matter and quadrupled in grey matter.

In summary, capillaries were initially sparse in the early post-natal mouse spinal cord, but equally distributed throughout grey and white matter regions. There was a subsequent significant increase in both the size and ramification of capillaries during the first 3 weeks of post-natal development, superseding the growth of the spinal cord, and was most notable in grey matter (where motor neuron cell bodies are located).

Capillary density in spinal cord is dramatically decreased in Taiwanese SMA mice

When we repeated the analyses of spinal cord vasculature on litters of Taiwanese SMA mice, it was immediately apparent, from images of stained capillaries in whole spinal cord, that there was a marked decrease in capillary density in SMA compared to control littermates at P11. At this late symptomatic stage, capillaries were still sparse in the spinal cord of SMA mice, leaving considerable distances between neighboring vessels. Little of the expected differentiation between white and grey matter was apparent in SMA mice compared to that observed in littermate control mouse spinal cords (Fig 4A,B), including the ventral grey horn. This finding suggested that capillary density had not significantly increased in the region of spinal cord containing lower motor neuron cell bodies over this period in SMA. A subsequent temporal analysis revealed that capillaries were equally sparse in both SMA and control mouse spinal cords at birth, and had not increased in SMA by P5, resulting in a significantly hypovascular appearance (Fig 4C). By P11, SMA spinal cords were less than half as capillary-dense as control littermates (Fig 4C), with segmentation of dorsal and ventral grey and white matter revealing that all territories of the spinal cord were similarly depleted (Fig 4D-G).

In summary, capillary density did not increase in SMA mouse spinal cord between P3 (pre-symptomatic) and P11 (late-symptomatic) stages. Capillary growth in mouse spinal cord occurs by sprouting angiogenesis, suggesting a defect in this process when SMN levels are reduced. Such post-natal developmental hypovascularity would likely lead to increased diffusion distances between capillaries and motor neurons in the ventral grey horn.

Significant vascular deficiency of spinal cord is replicated in a second mouse model of severe SMA

We were keen to determine if these significant vascular defects were epiphenomena specific to *SMN* gene manipulation in the Taiwanese SMA model mouse, or rather represented a common feature of neuromuscular pathology in mouse models of severe SMA. Therefore, we turned to another commonly used and well characterized mouse model of SMA (Δ7 mice [23]). We chose P14 as a direct comparison with the P11 data from the Taiwanese model, representing a late symptomatic time-point [3, 24-26]. In these slightly older mice the differential capillary density between grey and white matter is more apparent in both control and SMA spinal cords. Capillary density was quantified in an identical manner, and significant decreases were seen in each region and territory of the spinal cord in SMA compared to littermate controls (data not shown). Pooling the data for all regions, for this second mouse model of severe SMA, we found the same pronounced and significant decrease in capillary density in SMA spinal cord (Fig 4H-J). In fact the relative capillary density in P14 Δ7 mice is remarkably similar to that in the younger

P11 Taiwanese mice. In each case this density appears to have been maintained and to not have increased since the early post-natal period.

Taken together, these data suggest that a pronounced post-natal, developmental capillary deficiency is a robust and repeatable consequence of SMN depletion in mouse spinal cord. When considered alongside the reproducible capillary defects observed in skeletal muscle, we suggest that SMN depletion leads to widespread defects in post-natal angiogenesis. Significantly, these two affected tissues encompass both the somatic and synaptic (neuromuscular junction) fields of lower motor neurons.

Depleted vasculature results in significant in vivo hypoxia in spinal cord of severe Taiwanese SMA mice

The sparse capillary bed observed in SMA spinal cord resulted in increased diffusion distances between motor neurons and their capillaries (Fig5 A). A key question to address was whether this vascular phenotype had any impact upon the oxygenation/hypoxia status of lower motor neuron cell bodies in SMA. In order to test this we used a technique where hypoxic cells can be tagged *in vivo* and later identified after sacrifice using pimonidazole hydrochloride (PIMO). PIMO binds to thiol residues in cells with an oxygen concentration less than 14 µM which is equivalent to an oxygen tension <10 mm Hg at 37°C [27]. Physiological oxygen tension differs depending on the body tissue, but a value >35 mm Hg in the brain is considered sufficient to ensure normal oxygenation [28]. PIMO labeling therefore indicates oxygenation levels <30% that in the healthy CNS.

P5 Taiwanese severe SMA mice were chosen for PIMO-dosing and sacrifice, as it represents a pre/ early symptomatic time-point, at which vascular defects were present, but the mice remained generally healthy (at this age SMA mice are virtually indistinguishable from their healthy littermates in our hands). We double-labeled spinal cord to allow parallel visualization and quantification of Nissl-positive neurons and DAB-positive hypoxic cells. In control, non-PIMO injected staining experiments no DAB-positive (hypoxic) cells were present in spinal cord (data not shown). This demonstrated both the efficacy of the technique and the absence of subsequent false positive results in PIMO-dosed mice. Control littermates injected with PIMO showed very few cells with a positive PIMO-antibody reaction, indicating very little tissue hypoxia (Fig 5B). However, in striking contrast, PIMO-positive cells were widely distributed throughout the spinal cord, many of which were neurons, being co-stained for Nissl substance (Fig 5B). DAB positive tissue has been thresholded and highlighted to demonstrate areas of tissue hypoxia (Fig5 C). Quantification of DAB and Nissl co-positive large neurons in the ventral gray horn (representing lower motor neurons) indicated a significant (>3 fold) increase in hypoxic neurons in the spinal cord of Taiwanese SMA mice compared to control littermates (Fig 5D).
In summary, spinal cord, and in particular lower motor neuron soma, were hypoxic at early symptomatic time-points in severe SMA mice. This finding demonstrates that the depleted vasculature phenotype in SMA mice leads to functional hypoxia in clinically-relevant tissue and may therefore provide an additional pathway through which the neuromuscular system is rendered vulnerable in SMA.

The blood-spinal cord barrier is defective in SMA mice

Hypoxia will have direct effects upon motor neurons, but in addition may result in secondary changes in spinal cord, which could further damage motor neurons. Hypoxia can trigger changes in the blood brain barrier (BBB) [29], and leaky BBB and blood spinal cord barriers (BSCB) have been shown to lead to direct damage of motor neurons [30]. Therefore we set out to determine if the BSCB showed any signs of damage in SMA spinal cord [31]. We examined 3 core elements of the BSCB; the tight-junctional proteins claudin-5 (CL-5) and zona occludens-1 (ZO-1) found on endothelial cells, and the water transporter aquaporin-4 (AQ-4) found on astrocytes. At P11, ZO-1 was closely co-localised with GSL-1 positive blood vessels, and AQ-4 was also associated with all vessels examined in SMA mouse spinal cord. In contrast, CL-5 showed a very heterogeneous distribution in SMA mice. Here, many vessels showed close co-localisation, but many were negative for CL-5 (Fig 6). Given that hypoxia is known to affect CL-5 accumulation, we suggest that these changes in the BSCB occur downstream of spinal cord hypoxia. It is therefore likely, that an incomplete BSCB barrier will further amplify motor neuron damage in SMA.

In summary the BSCB was impaired in SMA mouse spinal cord, thereby identifying an additional, indirect and negative consequence of abnormal vascular development, that could contribute directly to motor neuron pathology in SMA.

Discussion

We can no longer view SMA as a disease that solely and specifically affects 'vulnerable' motor neurons. Evidence now points to significant systemic defects in SMA, but as both motor neurons and skeletal muscles are early and key targets of SMA, we need to better understand how SMN-depletion within these cell types can impact on the development and survival of the neuromuscular system.

This study has revealed significant defects in the development and post-natal maturation of capillary beds in SMA disease-relevant, proximal skeletal muscle and spinal cord in the first couple of post-natal weeks in severe SMA mice. Importantly, we show that similar vascular defects are also present in severe SMA patient muscle biopsies. Significantly, we build on these findings to demonstrate that vascular defects in SMA lead to *in vivo* hypoxia of spinal cord (including lower motor neuron soma) at an early symptomatic time-point. In addition to the gross defects in vascular development, defects in key BSCB proteins are also present in SMA mouse spinal cord. Given the known sensitivity of lower motor neurons to hypoxia *in vivo* [32], these findings highlight a novel link between systemic vascular pathology and the particular vulnerability of the neuromuscular system in SMA. This novel description of vascular defects in severe forms of SMA, suggests that therapeutic targeting of the vascular system in order to ameliorate functional hypoxia and BSCB defects is likely to be required in order to deliver a systemic rescue of SMA.

Skeletal muscle capillary beds fail to develop normally in the early post-natal period

In SMA proximal skeletal muscle, capillary density, calculated using either a measure of capillary density per unit area or number of capillaries per muscle fiber profile, was less than half that in control littermates (Fig 1C,D). Diffusion distances were therefore increased and many individual fibers were no longer immediately adjacent to a capillary (Fig 1B). The number of small, presumed angiogenic, capillaries was most severely affected, but larger, intramuscular arterioles expressing α-SMActin appeared to some extent spared in skeletal muscle (Fig 1E). We have previously shown that skeletal muscle capillary beds appear normal at birth [12], suggesting that vessels present at birth remain, mature normally, and are largely unaffected by disease progression, but that small vessels undergoing active angiogenesis as the animal grows, are most affected. Most importantly, the capillary bed is severely compromised and diffusion distances to both muscle fibers and nerve terminals at neuromuscular junctions are increased. We have previously shown that neonatal mouse neuromuscular junctions are surprisingly resistant to hypoxic injury, but this resistance is rapidly lost after P10, leaving P21 mice very sensitive to even relatively short periods of hypoxic insult [33]. Further, hypoxia-reperfusion injury as occurs when the quality of tissue perfusion oscillates produces profound injury to motor nerve terminals while leaving skeletal muscle fibers relatively unscathed [34]. The pathological presentation of these injuries is not dissimilar from the motor nerve terminal damage seen as one of the earliest pathological features in SMA [16]. A very recent report has shown that post-natal hypoxia significantly stunts growth and negatively modulates motor function [35]. Taken together, these studies point toward possible disease mechanisms.

Conserved vascular defects are present in human severe SMA patients and mouse models of severe SMA

We were keen to determine whether the data from the two mouse models of severe SMA accurately predicted vascular defects in SMA patients. Type I/II patient skeletal muscle biopsies showed muscle atrophy as expected (Fig 2B) [36], and given these differences in fiber size, the calculation of capillary: fibre ratio, as used here, is the most reliable indicator of overall muscle vascularity. This methodology indicated similar values at under 1 month of age (C:F = 0.1:1 in Control and 0.08:1 in SMA), but a tenfold difference in values at 33-36 months of age (C:F = 0.8:1 in Control and 0.08:1 in SMA). These data suggest that capillary beds are relatively normal at birth, but then fail to develop as the child grows, which exactly mirrors the data collected from the two mouse models of severe SMA, suggestive of a disruption of post-natal angiogenesis in SMA. This supports the concept of 'threshold pathology' in SMA, and the notion that therapies directed solely at the nervous system, may ultimately uncover additional non-neuronal pathologies [3]. This also further argues for the importance of systemic treatment approaches, particularly in severe SMA, as suggested by recent SMN viral delivery and oligonucleotide studies [9, 10]. Taken together, these data provide support for the idea that severe SMA mice are reliable models in which to study both the development and treatment of significant, vascular pathology in severe SMA patients.

Spinal cord capillary beds fail to develop normally in the early post-natal period

The pathological hallmark of SMA is the profound loss of spinal motor neurons. With this in mind, we investigated the blood supply of the spinal cord and showed that

capillaries fail to develop normally in severe SMA mice. They do not show the rapid increase in density, brought about by active angiogenesis, which occurs in white, and more strikingly, in grey matter in littermate controls. This results in SMA ventral grey matter having less than half the normal density of capillaries (Fig 4B,C). Embryonic development appears unaffected, as there are no differences at birth, rather a failure to develop in the postnatal period after birth is suggested. Specifically, growth of the capillary bed in SMA mice barely keeps pace with the growth of the spinal cord, resulting in a consistently low density. This contrasts with unaffected littermates where capillary growth outstrips spinal cord growth resulting in significantly increased density. Importantly, this is also the case in a second mouse model of SMA and specifically one generated using a different transgenic strategy to include the delta 7 transgene and thereby avoiding positional effects (Fig 4H,I).

This reduction in capillary density could contribute to the pathogenesis of SMA, particularly the degeneration of motor neurons. A 10-15% reduction in the total length and number of spinal cord capillaries results in a 30-45% reduction in spinal cord blood flow [37]. A similar decreased perfusion of the cord occurs rapidly subsequent to spinal cord injury [38], and leads to motor neuron degeneration [39].

Early symptomatic severe mouse SMA spinal cord is significantly hypoxic

Given the importance of oxygenation for cell survival, we directly measured hypoxia in early symptomatic spinal cord. In SMA, significant numbers of hypoxic cells were present throughout spinal cord, and specifically there was an increase in the number of hypoxic large, Nissl-positive (likely) motor neurons at this early symptomatic time-point in ventral spinal cord (Fig 5B,C,D). PIMO stain indicated oxygen concentrations

less than 30% of normal levels in the CNS. This tissue hypoxia was observed at an early stage in disease progression (P5), which is prior to or in-line with the appearance of neuromuscular pathology [25] [15]. Patient autopsies show markers of oxidative stress in the motor neurons and brains of SMA patients [40] and oxidative stress is a major cause of motor neuron death in clinically similar ALS [41, 42]. PIMO is rapidly cleared from the body by urinary excretion and therefore kidney function in SMA mice is a relevant consideration. Only one study has directly assessed renal function in the Taiwanese severe mouse model, and they found no significant differences in two key markers of renal function: urea nitrogen and creatinine in blood [43]. We therefore conclude that it is unlikely that altered renal function has biased our interpretation of PIMO data in SMA mouse spinal cord.

The final form of the normal vascular system is widely considered to be barely sufficient for the functioning of a healthy CNS [44] and given the relatively high metabolic needs of the CNS [45], the likely effects of chronic hypoxia due to hypovascularity are significant. Deletion of the hypoxia response element in mice, diminished vascular perfusion and triggered degeneration of 30% of ventral horn motor neurons [39]. These mice presented with severe muscle weakness and an ALS-phenotype with hindlimb clasping, muscle weakness and progressive immobility [39]. Hypoxia is therefore demonstrated to be a risk factor in triggering motor neuron degeneration, and likely contributes to motor pathology in SMA.

Spinal cord hypoxia is predicted to have additional, negative effects on disease progression

Aside from obvious deleterious effects on cell metabolism and survival, hypoxia also has a negative effect upon *SMN* splicing, by increasing levels of exon 7 skipping in the *SMN2* gene [46], which would be expected to result in further depletion of SMN levels in hypoxic tissue. This suggests that hypoxia could be a major modulator of SMN protein levels, the main determinant of disease severity [47]. Furthermore it has been shown that reactive oxygen species, generated during hypoxia, inhibit SMN complex activity in a dose-dependent manner; specifically it is proposed that SMNΔ7, the major protein product of *SMN2* may be particularly vulnerable to oxidative stress [48]. Major changes in gene transcription occur in the SMA late symptomatic spinal cord [49], suggestive of significant, ongoing developmental anomalies such as these. A situation may therefore exist whereby reduced SMN protein levels induce a hypoxic state due to morphological vascular defects, which in turn causes a reduction in SMN protein levels and further exacerbates disease progression.

The protein composition of the blood spinal cord barrier is defective in SMA mice

The blood brain barrier is key to maintain the 'protected' status of the CNS. In SMA only Claudin-5, a component of endothelial cell tight junctions, did not completely co-localise with blood vessels, particularly in smaller vessels (Fig 6), suggesting incomplete formation of the BSCB. Once again, this indicates a post-natal failure in development and maturation of blood vessels, where the smallest and presumed recently formed vessels do not acquire full barrier properties.

Mice maintained in hypoxic conditions develop a 41% decrease in Claudin-5 protein expression, in the blood retinal barrier, resulting in leakage [50]. We suggest that the

hypoxia we see at P5 has at least partly driven the defects observed in the BSCB at P11. The particular sensitivity of Claudin-5 to hypoxia could explain why it appears to be the only BSCB component affected in SMA. This could in turn be a factor in motor neuron damage resulting via a leaky BSCB [30].

Changing perceptions

SMA has traditionally been viewed as a disease of lower motor neurons, with the development of therapeutic interventions for many years focused on maintaining or replacing motor neurons [51], based on the concept that they are selectively vulnerable [16]. Our data suggest that hypoxia, driven by primary vascular defects, may contribute to this vulnerability. Here, motor neurons become highly active in the post-natal period and oxygen demand is not met by a defective vasculature, leading to metabolic failure and the production of oxygen radicals, which together result in motor neuron dysfunction and death. Added to this the negative effects of hypoxia on BSCB integrity and *SMN* splicing, produces a perfect storm of factors deleterious to motor neurons. Cardiovascular phenotypes, including cardiac muscle capillary defects, are now well documented in SMA with morphological and functional defects reported clinically and experimentally [5, 12, 52-54]. In addition, we have now shown significant vascular defects in patients with severe SMA. It is therefore possible that capillary defects could contribute to muscle wasting, motor neuron loss and the appearance of clinical symptoms, at least patients with severe SMA. This shift in perspective regarding the nature of SMA pathology has major implications for future therapeutic development.

Author contributions

ES, RDL, KH, JNS and HZ carried out the experiments, acquired and analysed the data.

SHP and THG designed the experiments.

SHP, THG, KT and FM analysed the data and wrote the manuscript.

Acknowledgements

SHP is funded by The Euan MacDonald Centre for Motor Neurone Disease Research and The SMA Trust. THG is funded by Muscular Dystrophy UK and The SMA Trust KT is funded by The SMA Trust and the Motor Neurone Disease Association. HZ is funded by National Institute for Health Research and Great Ormond Street Hospital Biomedical Research Centre and FM is funded by Medical Research Council and Great Ormond Street Hospital Charity. The MRC Centre for Neuromuscular Diseases BioBank London (CNMD_BBL) is gratefully acknowledged.

Potential conflicts of Interest

None of the other authors has any potential conflicts of interest.

Figure legends

Figure 1

Capillary density is reduced in the skeletal muscle of the proximal forelimbs of early symptomatic SMA mice

Representative micrographs of capillaries labeled with the endothelial cell marker *Griffonia simplicifolia* Lectin-1 (GSL-1: [55] red), in transverse sections of proximal forelimb muscle from P8 Taiwanese in (A) control and (B) SMA mice. (C) Quantification of capillary density expressed as a percentage of cross-sectional muscle area showed that SMA muscle was significantly less capillary-dense (2.97%) compared with control mice (6.22% *** P<0.001 unpaired, two-tailed *t*-test). (D) Alternatively, calculating the ratio of capillaries to muscle fiber profiles in transverse sections of whole proximal forelimbs (mean ± s.e.m.) confirmed and extended our findings, demonstrating a significantly decreased (<40%) capillary/muscle fiber ratio in SMA mice (0.25) compared with control littermates (0.68: *** P<0.001 unpaired, two-tailed *t*-test). *n*≥3 mice and *n*≥250 muscle cross sections per group. (E) The number of intra-muscular arterioles (defined as vessels expressing α-SMActin) appeared reduced in SMA mice. We counted the number of intra-muscular vessels expressing α-SMActin in transverse-sections of whole proximal forelimb. There was a significant (~57%) decrease in the mean number of intra-muscular arterioles: 33.6 vessels/section in control mice to 14.3 vessels/section in SMA mice (***P<0.001 unpaired, two-tailed *t*-test).

Scale bar = 50μm

Figure 2

Capillary density is reduced in skeletal muscle biopsies from severe SMA patients

We obtained skeletal muscle biopsies from diagnostically confirmed severe SMA patients and control individuals with no vascular or neuromuscular disease. These were processed for immunocytochemistry and capillary: fibre ratio calculated, as for mouse experiments. Muscles were co-stained with laminin to reveal muscle fibre profiles and PECAM 1 to show blood vessels. (A) Control muscle (25 mo) shows a typical young/ juvenile arrangement, where each capillary is close to 1-2 muscle fibres, resulting in a mean capillary: fibre ratio of 0.78:1. (B) SMA muscle (24 mo) shows a decreased number of capillaries, resulting in most muscle fibres being more distant from a capillary, and a mean capillary: fibre ratio of 0.08:1. (C) Data from a range of control children (mean ±SEM) and SMA patients reveals a steady increase in vascularity in normal controls, but a failure to effectively vascularize in SMA over a 36 month period. Regression analysis of the slope of change in vascularity with increasing age, indicated that there was a significant difference between control and SMA muscle biopsies.

n=9 Control, n=7 SMA patients and 3-9 (mean=5) sections per patient.*** $P<0.001$, Scale bar A = 25µm

Figure 3

Spinal cord capillary bed density increases from birth to 3 weeks post-natal in wild-type spinal cord

Counts of capillary density in C57Bl wild-type mice were pooled from left and right spinal cord hemisections, as they were not significantly different. There were also no significant differences between thoracic and limb-regions of the spinal cord, and all the following data are drawn from thoracic spinal cord. (A) Capillary density assessed by quantitation of PECAM-1 immunostaining in C57Bl wild-type mice between P3-P21. Bars represent mean ± s.e.m. The total capillary density of the spinal cord significantly increased between each age (one-way ANOVA with Tukey post-hoc test: ***P<0.001). Each bar represents data from 3 mice, ≥30 sections and ≥480 fields of view. (B) Scatter plots show a significant increase (~15%) in capillary caliber between P3 and P21 (unpaired two tailed *t*-test: ***P<0.001). *n*=3 mice and ≥500 capillary profiles for each time-point. (C) Differentiation of grey (black bars) and white (white bars) matter in dorsal (D) and ventral (V) regions of spinal cord using cresyl violet revealed that grey matter becomes significantly more capillary-dense than white matter over time (one-way ANOVA and Tukey post-hoc test: ***P<0.001. *n*=3 mice per age group and ≥30 sections per time-point.

Figure 4

Capillary density is depleted in SMA spinal cord

Representative montage micrographs of sections from Taiwanese P11 (A) control and (B) SMA spinal cord visualised with PECAM 1 (shown black) in Taiwanese severe SMA mice. Individual images used to construct the montages were taken at 10x magnification. (C) Bar chart (mean ± s.e.m.) of quantification of capillary density in the spinal cord from P0 to P11 in Taiwanese control littermates and SMA mice. One-way ANOVA with Tukey post-hoc test: NS P>0.05; ***P<0.001. *n*≥3 mice and *n*≥3 spinal cords for each bar. (D,E,F,G) Capillary density is reduced in all four spinal cord regions and in both grey and white matter in P11 Taiwanese SMA mice. Bar charts (mean + s.e.m.) show quantification of capillary density in the spinal cord of P11 Taiwanese SMA mice and control littermates. Unpaired, two-tailed *t*-test: **P<0.01; ***P<0.001. *n*≥3 mice and *n*≥3 cords for each bar. (H) Representative montage micrograph of P14 control and (I) SMA spinal cord capillary bed visualised with PECAM-1 in SMNΔ7 mice. Individual images used to construct montage are 10x magnification. (J) Bar chart (mean ± s.e.m.) quantification of overall spinal cord capillary density in P14 SMNΔ7 SMA mice and control littermates. White bars = control and black bars = SMA mice. Unpaired, two tailed *t*-test, ***P<0.001. *n*≥3 mice and *n*≥3 cords for each bar.

Scale bar = 200 µm.

Figure 5

Diffusion distances are increased and cells and tissue are hypoxic in the ventral horn of the spinal cord

The number of capillaries surrounding motor neurons is reduced in late symptomatic Taiwanese SMA mice. (A) Representative micrographs of motor neurons labelled with SM1-32 (green) and the capillary bed with PECAM 1 (red) in control and late symptomatic P11 Taiwanese SMA spinal cords. Images are 20x magnification. (B) Representative micrographs of DAB visualisation of PIMO-labelled hypoxic cells in ventral horn of P5 control littermates and early symptomatic Taiwanese SMA mice. A diaminobenzidine (DAB: brown) reaction product indicates cells which were in an environment of <10 mm Hg at the time of PIMO injection. Spinal cords were counterstained with cresyl fast violet. Images are 40x magnification. (C) To highlight the PIMO positive hypoxic cells, we have thresholded and inverted the images to demonstrate the increase in the number of hypoxic cells (white) in SMA spinal cord. (D) Quantification revealed significantly increased number of hypoxic cells in the ventral region of P5 Taiwanese SMA spinal cord. Bar chart (mean ± s.e.m.) of hypoxic cells (per unit area) in ventral horn of P5 control littermates (white bar), and symptomatic Taiwanese SMA mice (black bar). Unpaired, two-tailed *t*-test. ***P<0.001 $n \geq 3$ mice, $n \geq 3$ cords, $n \geq 27$ sections and $n \geq 54$ images for each bar. Scale bar = 50 µm.

Figure 6

The blood spinal cord barrier develops aberrantly in SMA spinal cord

Claudin-5 (CL-5) labelling is disrupted in P11 Taiwanese SMA mice, while aquaporin-4 (AQ-4) and zona occludens-1 (ZO-1) both appear normal. Representative micrographs of P11 Taiwanese SMA and control spinal cord visualised with GSL-1 to indicate capillaries (red) and co-labelled with AQ-4, CL-5 or ZO-1 (green). Arrowheads indicate capillaries negative for CL-5.

Scale bar = 50 µm.

References

1. Burghes AH, Beattie CE. Spinal muscular atrophy: why do low levels of survival motor neuron protein make motor neurons sick? Nature reviews Neuroscience. 2009 Aug;10(8):597-609.
2. Hamilton G, Gillingwater TH. Spinal muscular atrophy: going beyond the motor neuron. Trends Mol Med. 2013 Jan;19(1):40-50.
3. Sleigh JN, Gillingwater TH, Talbot K. The contribution of mouse models to understanding the pathogenesis of spinal muscular atrophy. Disease models & mechanisms. 2011 Jul;4(4):457-67.
4. Rudnik-Schoneborn S, Heller R, Berg C, et al. Congenital heart disease is a feature of severe infantile spinal muscular atrophy. J Med Genet. 2008 Oct;45(10):635-8.
5. Rudnik-Schoneborn S, Vogelgesang S, Armbrust S, Graul-Neumann L, Fusch C, Zerres K. Digital necroses and vascular thrombosis in severe spinal muscular atrophy. Muscle Nerve. 2010 Jul;42(1):144-7.
6. Paez-Colasante X, Seaberg B, Martinez TL, Kong L, Sumner CJ, Rimer M. Improvement of neuromuscular synaptic phenotypes without enhanced survival and motor function in severe spinal muscular atrophy mice selectively rescued in motor neurons. PLoS ONE. 2013;8(9):e75866.
7. Lee AJ, Awano T, Park GH, Monani UR. Limited phenotypic effects of selectively augmenting the SMN protein in the neurons of a mouse model of severe spinal muscular atrophy. PLoS ONE. 2012;7(9):e46353.
8. Wishart TM, Mutsaers CA, Riessland M, et al. Dysregulation of ubiquitin homeostasis and beta-catenin signaling promote spinal muscular atrophy. J Clin Invest. 2014 Apr 1;124(4):1821-34.
9. Hua Y, Liu YH, Sahashi K, Rigo F, Bennett CF, Krainer AR. Motor neuron cell-nonautonomous rescue of spinal muscular atrophy phenotypes in mild and severe transgenic mouse models. Genes Dev. 2015 Jan 12.
10. Zhou H, Meng J, Marrosu E, Janghra N, Morgan J, Muntoni F. Repeated low doses of morpholino antisense oligomer: an intermediate mouse model of spinal muscular atrophy to explore the window of therapeutic response. Hum Mol Genet. 2015 Aug 11.
11. Osborne M, Gomez D, Feng Z, et al. Characterization of behavioral and neuromuscular junction phenotypes in a novel allelic series of SMA mouse models. Hum Mol Genet. 2012 Oct 15;21(20):4431-47.
12. Somers E, Stencel Z, Wishart TM, Gillingwater TH, Parson SH. Density, calibre and ramification of muscle capillaries are altered in a mouse model of severe spinal muscular atrophy. Neuromuscul Disord. 2012 Dec 7;22:435-42.
13. Bell RD, Winkler EA, Singh I, et al. Apolipoprotein E controls cerebrovascular integrity via cyclophilin A. Nature. 2012 May 24;485(7399):512-6.
14. Anand A, Thakur K, Gupta PK. ALS and oxidative stress: the neurovascular scenario. Oxidative medicine and cellular longevity. 2013;2013:635831.
15. Riessland M, Ackermann B, Foerster A, et al. SAHA ameliorates the SMA phenotype in two mouse models for spinal muscular atrophy. Hum Mol Genet. 2010 Apr 15;19(8):1492-506.

16. Murray LM, Comley LH, Thomson D, Parkinson N, Talbot K, Gillingwater TH. Selective vulnerability of motor neurons and dissociation of pre- and post-synaptic pathology at the neuromuscular junction in mouse models of spinal muscular atrophy. Hum Mol Genet. 2008 Apr 1;17(7):949-62.
17. Sleigh JN, Barreiro-Iglesias A, Oliver PL, et al. Chondrolectin affects cell survival and neuronal outgrowth in in vitro and in vivo models of spinal muscular atrophy. Hum Mol Genet. 2014 Feb 15;23(4):855-69.
18. Saunders MI, Anderson PJ, Bennett MH, et al. The clinical testing of Ro 03-8799--pharmacokinetics, toxicology, tissue and tumor concentrations. Int J Radiat Oncol Biol Phys. 1984 Sep;10(9):1759-63.
19. Gualtieri F, Marinelli C, Longo D, et al. Hypoxia markers are expressed in interneurons exposed to recurrent seizures. Neuromolecular Med. 2013 Mar;15(1):133-46.
20. Walton MI, Bleehen NM, Workman P. Effects of localised tumour hyperthermia on pimonidazole (Ro 03-8799) pharmacokinetics in mice. Br J Cancer. 1989 May;59(5):667-73.
21. Zoladz JA, Semik D, Zawadowska B, et al. Capillary density and capillary-to-fibre ratio in vastus lateralis muscle of untrained and trained men. Folia Histochem Cytobiol. 2005;43(1):11-7.
22. Eliason G, Abdel-Halim SM, Piehl-Aulin K, Kadi F. Alterations in the muscle-to-capillary interface in patients with different degrees of chronic obstructive pulmonary disease. Respir Res. 2010;11:97.
23. Monani UR, Coovert DD, Burghes AH. Animal models of spinal muscular atrophy. Hum Mol Genet. 2000 Oct;9(16):2451-7.
24. Le TT, Pham LT, Butchbach ME, et al. SMNDelta7, the major product of the centromeric survival motor neuron (SMN2) gene, extends survival in mice with spinal muscular atrophy and associates with full-length SMN. Hum Mol Genet. 2005 Mar 15;14(6):845-57.
25. Hsieh-Li HM, Chang JG, Jong YJ, et al. A mouse model for spinal muscular atrophy. Nat Genet. 2000 Jan;24(1):66-70.
26. Monani UR, Sendtner M, Coovert DD, et al. The human centromeric survival motor neuron gene (SMN2) rescues embryonic lethality in Smn(-/-) mice and results in a mouse with spinal muscular atrophy. Hum Mol Genet. 2000 Feb 12;9(3):333-9.
27. Kizaka-Kondoh S, Konse-Nagasawa H. Significance of nitroimidazole compounds and hypoxia-inducible factor-1 for imaging tumor hypoxia. Cancer Sci. 2009 Aug;100(8):1366-73.
28. Carreau A, El Hafny-Rahbi B, Matejuk A, Grillon C, Kieda C. Why is the partial oxygen pressure of human tissues a crucial parameter? Small molecules and hypoxia. J Cell Mol Med. 2011 Jun;15(6):1239-53.
29. Belayev L, Busto R, Zhao W, Ginsberg MD. Quantitative evaluation of blood-brain barrier permeability following middle cerebral artery occlusion in rats. Brain Res. 1996 Nov 11;739(1-2):88-96.
30. Garbuzova-Davis S, Hernandez-Ontiveros DG, Rodrigues MC, et al. Impaired blood-brain/spinal cord barrier in ALS patients. Brain Res. 2012 Aug 21;1469:114-28.
31. Abbott NJ, Patabendige AA, Dolman DE, Yusof SR, Begley DJ. Structure and function of the blood-brain barrier. Neurobiol Dis. 2010 Jan;37(1):13-25.

32. Kim SM, Kim H, Lee JS, et al. Intermittent hypoxia can aggravate motor neuronal loss and cognitive dysfunction in ALS mice. PLoS ONE. 2013;8(11):e81808.
33. Murray LM, Comley LH, Gillingwater TH, Parson SH. The response of neuromuscular junctions to injury is developmentally regulated. FASEB J. 2011;EPub (15th January).
34. Baxter B, Gillingwater TH, Parson SH. Rapid loss of motor nerve terminals following hypoxia-reperfusion injury occurs via mechanisms distinct from classic Wallerian degeneration. J Anat. 2008 Jun;212(6):827-35.
35. Watzlawik JO, Kahoud RJ, O'Toole RJ, et al. Abbreviated exposure to hypoxia is sufficient to induce CNS dysmyelination, modulate spinal motor neuron composition, and impair motor development in neonatal mice. PLoS ONE. 2015;10(5):e0128007.
36. Byers RK, Banker BQ. Infantile muscular atrophy. Arch Neurol. 1961 Aug;5:140-64.
37. Zhong Z, Deane R, Ali Z, et al. ALS-causing SOD1 mutants generate vascular changes prior to motor neuron degeneration. Nat Neurosci. 2008 Apr;11(4):420-2.
38. Means ED, Anderson DK, Nicolosi G, Gaudsmith J. Microvascular perfusion experimental spinal cord injury. Surg Neurol. 1978 Jun;9(6):353-60.
39. Oosthuyse B, Moons L, Storkebaum E, et al. Deletion of the hypoxia-response element in the vascular endothelial growth factor promoter causes motor neuron degeneration. Nat Genet. 2001 Jun;28(2):131-8.
40. Hayashi M, Araki S, Arai N, et al. Oxidative stress and disturbed glutamate transport in spinal muscular atrophy. Brain Dev. 2002 Dec;24(8):770-5.
41. Beal MF, Ferrante RJ, Browne SE, Matthews RT, Kowall NW, Brown RH, Jr. Increased 3-nitrotyrosine in both sporadic and familial amyotrophic lateral sclerosis. Ann Neurol. 1997 Oct;42(4):644-54.
42. Barber SC, Mead RJ, Shaw PJ. Oxidative stress in ALS: a mechanism of neurodegeneration and a therapeutic target. Biochim Biophys Acta. 2006 Nov-Dec;1762(11-12):1051-67.
43. Liu HC, Ting CH, Wen HL, et al. Sodium vanadate combined with L-ascorbic acid delays disease progression, enhances motor performance, and ameliorates muscle atrophy and weakness in mice with spinal muscular atrophy. BMC medicine. 2013;11:38.
44. Dommisse GF. The blood supply of the spinal cord. A critical vascular zone in spinal surgery. J Bone Joint Surg Br. 1974 May;56(2):225-35.
45. Herculano-Houzel S. Scaling of brain metabolism with a fixed energy budget per neuron: implications for neuronal activity, plasticity and evolution. PLoS ONE. 2011;6(3):e17514.
46. Bebee TW, Dominguez CE, Samadzadeh-Tarighat S, Akehurst KL, Chandler DS. Hypoxia is a modifier of SMN2 splicing and disease severity in a severe SMA mouse model. Hum Mol Genet. 2012 Oct 1;21(19):4301-13.
47. Feldkotter M, Schwarzer V, Wirth R, Wienker TF, Wirth B. Quantitative analyses of SMN1 and SMN2 based on real-time lightCycler PCR: fast and highly reliable carrier testing and prediction of severity of spinal muscular atrophy. Am J Hum Genet. 2002 Feb;70(2):358-68.
48. Wan L, Ottinger E, Cho S, Dreyfuss G. Inactivation of the SMN complex by oxidative stress. Mol Cell. 2008 Jul 25;31(2):244-54.

49. Baumer D, Lee S, Nicholson G, et al. Alternative splicing events are a late feature of pathology in a mouse model of spinal muscular atrophy. PLoS Genet. 2009 Dec;5(12):e1000773.
50. Koto T, Takubo K, Ishida S, et al. Hypoxia disrupts the barrier function of neural blood vessels through changes in the expression of claudin-5 in endothelial cells. Am J Pathol. 2007 Apr;170(4):1389-97.
51. Greensmith L, Vrbova G. Possible strategies for treatment of SMA patients: a neurobiologist's view. Neuromuscul Disord. 1995 Sep;5(5):359-69.
52. Bevan AK, Hutchinson KR, Foust KD, et al. Early heart failure in the SMN{Delta}7 model of spinal muscular atrophy and correction by postnatal scAAV9-SMN delivery. Hum Mol Genet. 2010 Jul 28.
53. Heier CR, Satta R, Lutz C, Didonato CJ. Arrhythmia and cardiac defects are a feature of spinal muscular atrophy model mice. Hum Mol Genet. 2010 Aug 18.
54. Shababi M, Habibi J, Yang HT, Vale SM, Sewell WA, Lorson CL. Cardiac defects contribute to the pathology of spinal muscular atrophy models. Hum Mol Genet. 2010 Aug 17.
55. Laitinen L. Griffonia simplicifolia lectins bind specifically to endothelial cells and some epithelial cells in mouse tissues. Histochem J. 1987 Apr;19(4):225-34.

Figure 1

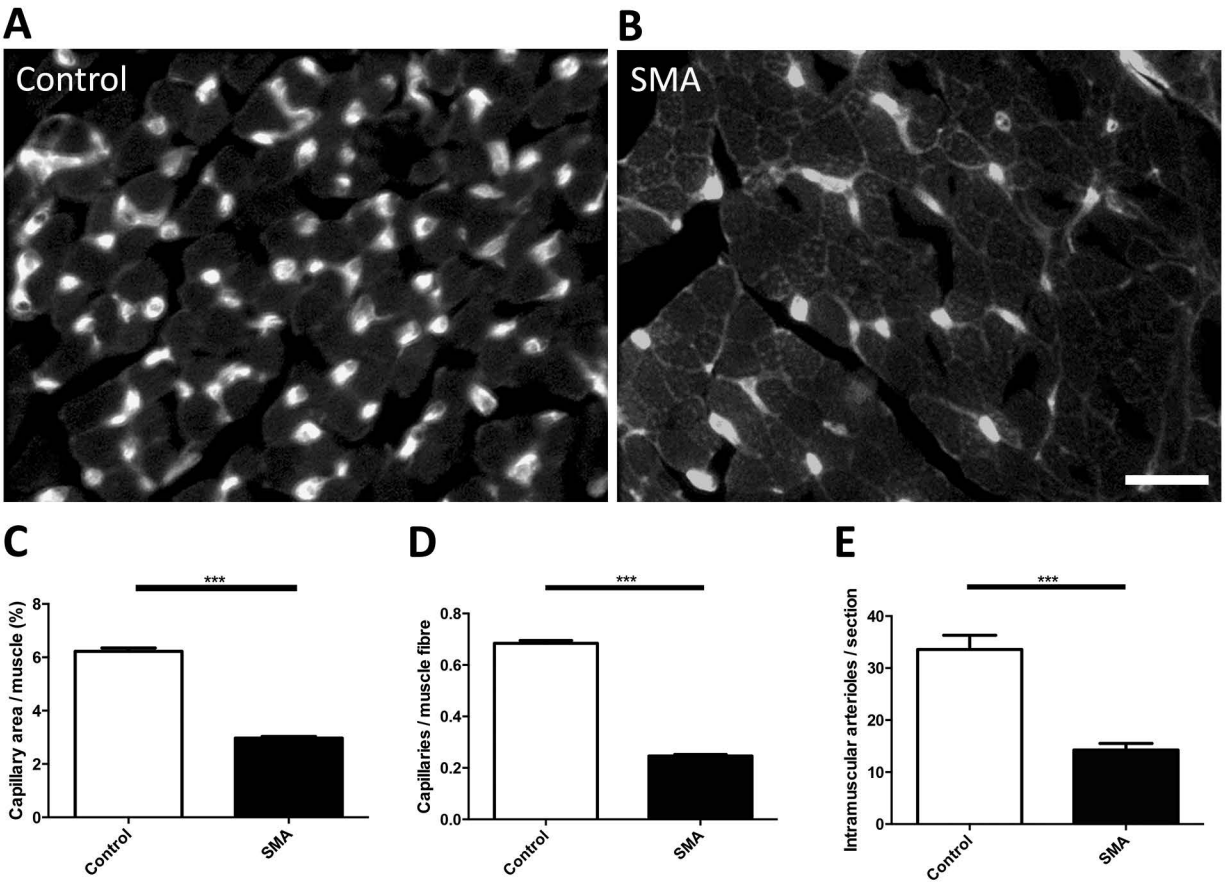
A
Control
B
SMA
C
***
Capillary area / muscle (%)
0
2
4
6
8
Control
SMA
D
***
Capillaries / muscle fibre
0.0
0.2
0.4
0.6
0.8
Control
SMA
E
***
Intramuscular arterioles / section
0
10
20
30
40
Control
SMA

Figure 2

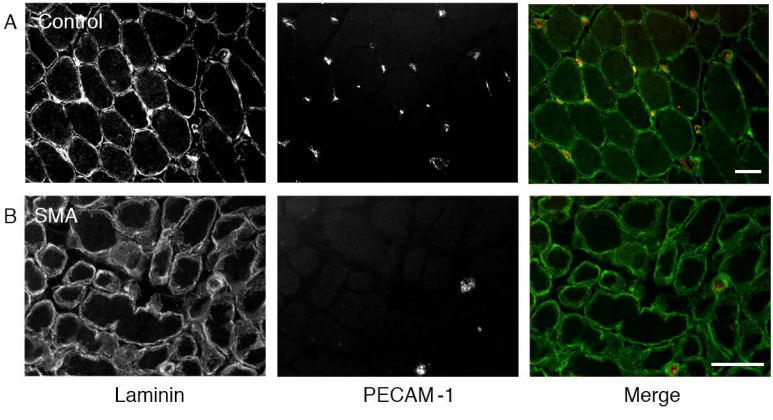
A
Control
B
SMA
Laminin
PECAM-1
Merge

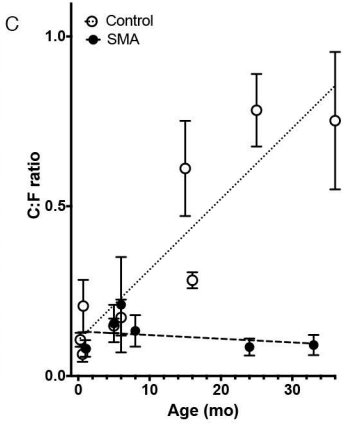
C
Control
SMA
C:F ratio
1.0
0.5
0.0
0
10
20
30
Age (mo)

Figure 3

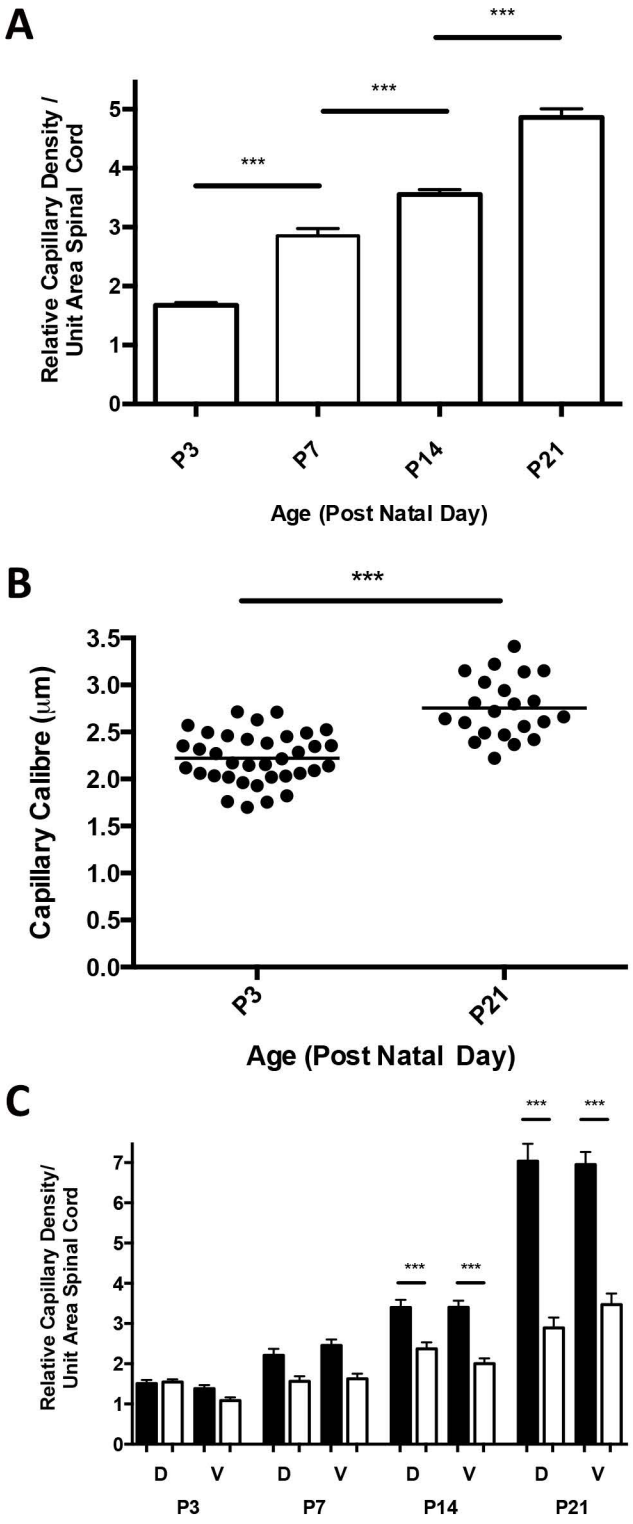
A
***
***
***
Relative Capillary Density / Unit Area Spinal Cord
0
1
2
3
4
5
P3
P7
P14
P21
Age (Post Natal Day)
B
***
Capillary Calibre (μm)
0.0
0.5
1.0
1.5
2.0
2.5
3.0
3.5
P3
P21
Age (Post Natal Day)
C
***
***
***
***
Relative Capillary Density/ Unit Area Spinal Cord
0
1
2
3
4
5
6
7
D
V
D
V
D
V
D
V
P3
P7
P14
P21

Figure 4

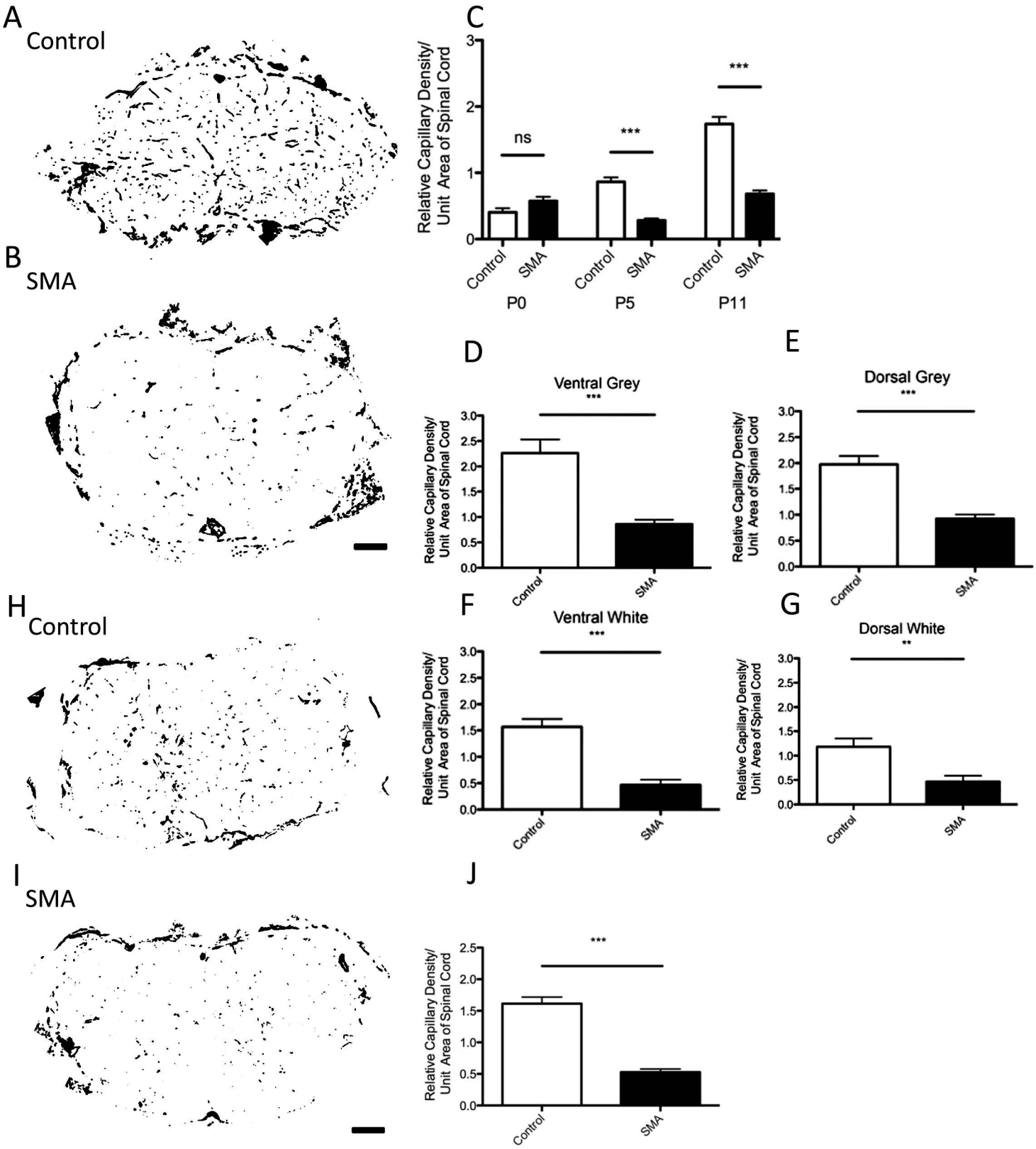
A
Control
B
SMA
C
Relative Capillary Density/ Unit Area of Spinal Cord
ns
***
***
Control
SMA
Control
SMA
Control
SMA
P0
P5
P11
D
Ventral Grey
***
E
Dorsal Grey
***
H
Control
F
Ventral White
***
G
Dorsal White
**
I
SMA
J
***

Figure 5

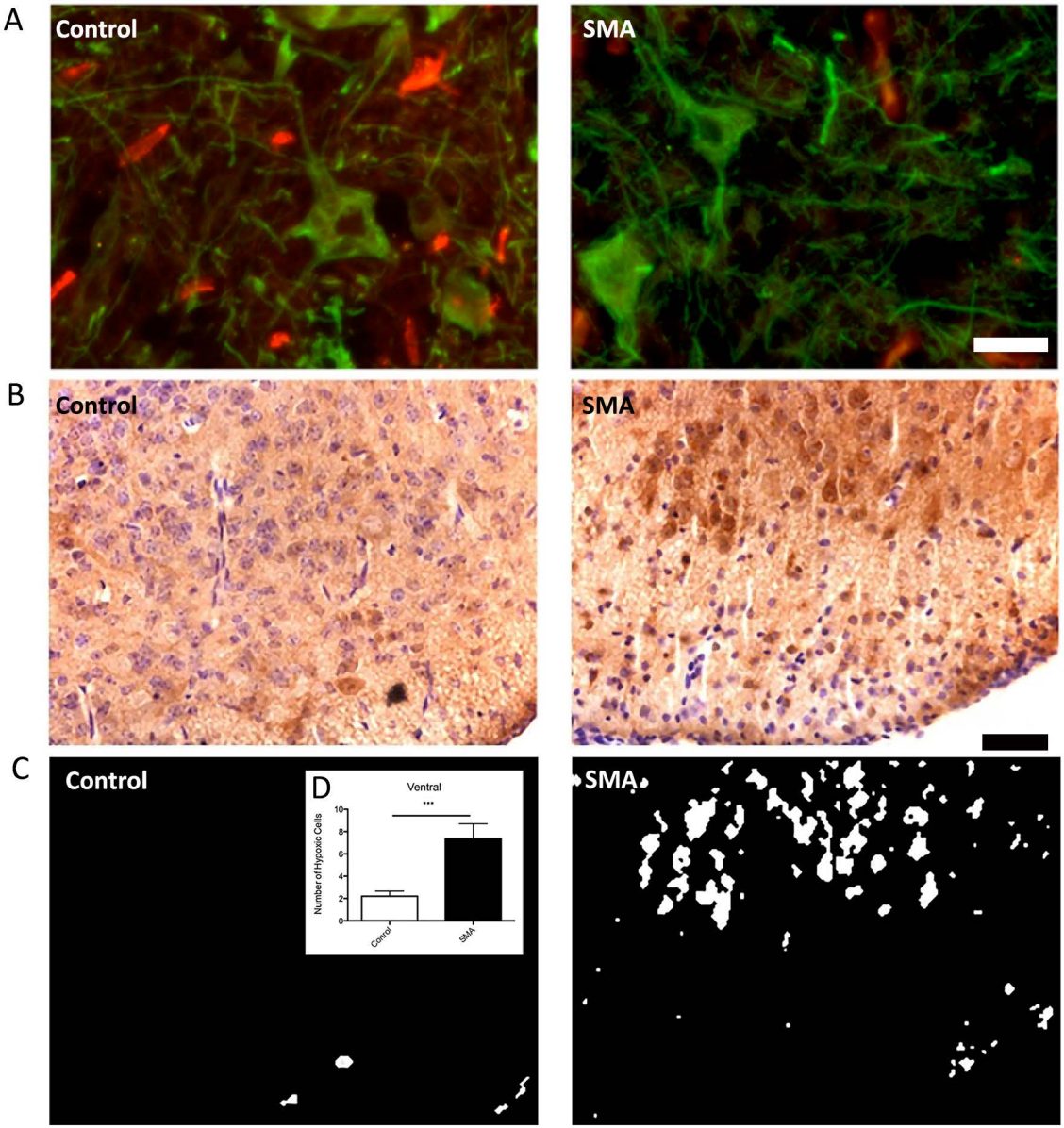
A
Control
SMA
B
Control
SMA
C
Control
D
Ventral
***
Number of Hypoxic Cells
10
8
6
4
2
0
Control
SMA
SMA

Figure 6